35th Annual International Conference of the IEEE EMBS
Osaka, Japan, 3 - 7 July, 2013

The Role of Topography in the Transformation of Spatiotemporal Patterns by a Large-Scale, Biologically Realistic Model of the Rat Dentate Gyrus

Gene J. Yu, *Student Member*, *IEEE*, Phillip J. Hendrickson, *Member*, *IEEE*, Brian S. Robinson, *Student Member*, *IEEE*, Dong Song, *Member*, *IEEE*, and Theodore W. Berger, *Fellow, IEEE*

***Abstract*—A large-scale, biologically realistic, computational model of the rat hippocampus is being constructed to study the input-output transformation that the hippocampus performs. In the initial implementation, the layer II entorhinal cortex neurons, which provide the major input to the hippocampus, and the granule cells of the dentate gyrus, which receive the majority of the input, are modeled. In a previous work, the topography, or the wiring diagram, connecting these two populations had been derived and implemented. This paper explores the consequences of two features of the topography, the distribution of the axons and the size of the neurons' axon terminal fields. The topography converts streams of independently generated random Poisson trains into structured spatiotemporal patterns through spatiotemporal convergence achievable by overlapping axon terminal fields. Increasing the axon terminal field lengths allowed input to converge over larger regions of space resulting in granule activation across a greater area but did not increase the total activity as a function of time as the number of targets per input remained constant. Additional simulations demonstrated that the total distribution of spikes in space depends not on the distribution of the presynaptic axons but the distribution of the postsynaptic population. Analyzing spike counts emphasizes the importance of the postsynaptic distribution, but it ignores the fact that each individual input may be carrying unique information. Therefore, a metric should be created that relates and tracks individual inputs as they are propagated and integrated through hippocampus.**

I. Introduction

The hippocampus converts short-term memory into long-term memory. We contend that, at a neural level, this re-encoding of short-term into long-term memory is implemented as a nonlinear transformation of spatiotemporal patterns originating in the entorhinal cortex (and earlier) into new, different representations, as memory-related activity propagates through the intrinsic pathways of the hippocampus, ultimately emerging as CA1/subicular activity.

In order to quantify the input-output characteristics of the hippocampus and its ability to convert short-term memory into long-term memory, we are constructing a large-scale, biologically realistic, computational model of the rat hippocampus. Because the rat hippocampus has been the most thoroughly studied, the model is defined by rodent constraints.

G. J. Yu, P. J. Hendrickson, B. S. Robinson, D. Song and T. W. Berger are with the Center for Neural Engineering, Department of Biomedical Engineering, University of Southern California, Los Angeles, CA 90089 USA (e-mail: geneyu@usc.edu; bsrobins@usc.edu; phendric@usc.edu; dsong@usc.edu; berger@bmsr.usc.edu)

Spatiotemporal patterns are the means by which neuron populations are known to communicate information. The spatiotemporal pattern describes which neurons are firing and at what time. A neuron gathers input triggered by action potentials from a region in space using dendrites, integrates the timing of inputs from that space, and fires an action potential at some time. Thus, an entire neuron population converts one spatiotemporal pattern into another.

Our model defines, using an anatomical and physiological basis, several properties to account for the realistic integration of inputs across time and space by a single neuron. Iterating these details across the vast number of presynaptic input cells and postsynaptic output cells in the system, the model attempts to recreate the transformation of the spatiotemporal pattern that the rat hippocampus could employ. This model-in-progress begins with the major input population to the hippocampus and the major receiver of that input, the entorhinal cortical (EC) layer II neurons and the granule cells (GCs) of the dentate gyrus.

This paper focuses on that which gives rise to the spatial aspect of spatiotemporal patterns by studying a property that is intertwined with the spatial pattern, the anatomical topography. The anatomical topography describes the physical connectivity between two neuron populations. Simply put, it is the wiring diagram. The wiring between the EC cells and the GC was determined using a set of constraints determined from anatomical data. The determination was described in a previous paper [1][2].

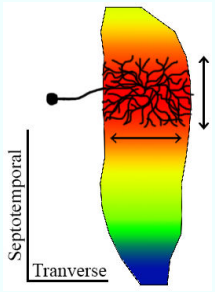

Figure 1. Two properties of topography. The shape of the dentate gyrus, the postsynaptic space, is depicted. The color map depicts the density of axonal projection across the dentate gyrus based on anatomical data with the highest density in red and the lowest in blue. An EC cell is represented with its axon terminal field drawn. Based on the literature, the width of the axon terminal field extends across the entire transverse axis of the dentate gyrus. In this study, the septotemporal (vertical) length is varied.

For the topography in the model, there are several major properties that define it. First, there is the relationship between the position of the presynaptic inputs and the position of their projections on the postsynaptic space. This determines what kind of information is projected to which population and at what intensity. The second property is the shape of the projection, the axon terminal field. The axon terminal field will further constrain the subset of the population with which the presynaptic neuron could potentially synapse. The definition of the axon terminal field will determine whether the projection is point-to-point or

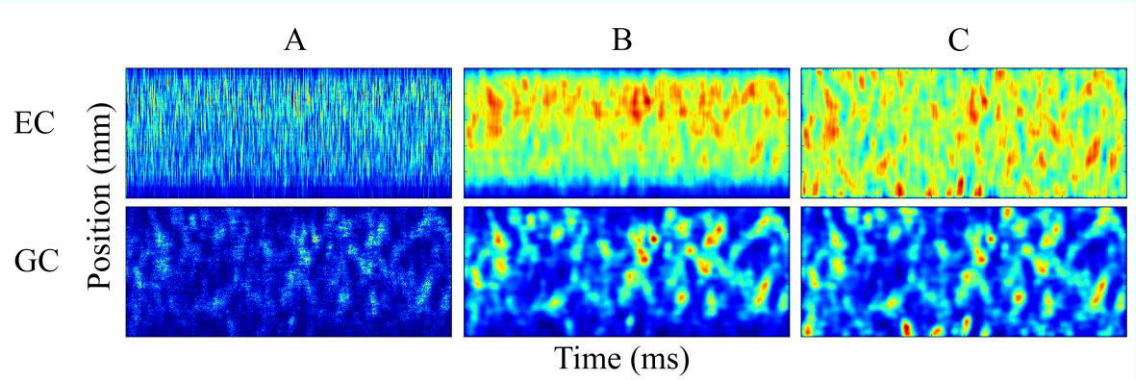

Figure 2. Comparison of EC cell activity and GC activity. The top row represents the EC cell based activation of GCs with the vertical position of the GCs on the y-axis and the time of the spike in the x-axis. The bottom row represents the firing of GCs. 500ms of data is shown. **A**. The spiking data before being convolved with a 2-D gaussian. **B**. The spiking data convolved with the gaussian. **C**. The spiking data convolved with a gaussian with each row normalized by the number of GCs present in that vertical extent.

whether it fans (Fig. 1). These properties change the area of activation across space, which should predominantly influence the spatial pattern. In this paper, both the distribution of the projections and the size of the axon terminal field are varied to investigate how these features of topography affect the spatiotemporal pattern.

II. Methods

A. Model Framework

The multi-compartmental granule cell models were coded with Python using NEURON as a module [3]. Using L-NEURON, unique morphologies were generated for each granule cell based on granule cell reconstructions. Hendrickson et. al. contains a more detailed look at the generation of morphology [4]. Attached to a soma, the dendrites were partitioned into a granule cell layer and the inner, middle, and outer thirds of the molecular layer. Voltage- and ion-gated membrane channels were also inserted and distributed throughout the morphologies based on the partitions mentioned above based on the model created by Santhakumar et. al. [5]. The granule cells were distributed along a dentate gyrus map following a density distribution that varied along both the vertical and horizontal axis of the dentate gyrus based on Gaarskjaer's work [6]. Each granule cell was given a range of spines, separate for the inner, middle, and outer third of the dendrites. Upon these spines, EC cells could synapse.

The entorhinal cortical layer II cells were modeled as spike generators to provide the input to the granule cells. Based on their distinct synaptic targets, the EC cells were separated into the lateral and medial entorhinal cortex (LEC and MEC). The LEC synapses onto the outer third of the granule cell dendrites, and the MEC synapses onto the middle third. The axon terminal fields of EC cells have been reported to extend across the entire transverse extent of the dentate gyrus, so only the septotemporal, or vertical, length was varied [7].

B. Simulation Parameters

6,600 MEC and 4,600 LEC cells were used as input. Each EC cell generated a random Poisson interspike interval train with a mean that was uniformly distributed between 1.5-3.5Hz for the MEC cells and between 3.5-8.0Hz for the LEC cells. Poisson-distributed intervals were used to provide broadband frequency input to the system. 100,000 granule cells were included in the model. These numbers were chosen to construct a $1/10^{th}$ scale of the full neuron population in the rat brain. EC cells modeled as independent, random Poisson spike train generators were connected to subsets of biologically realistic granule cell models based on the axon distribution and axon terminal field length. Each experiment simulated 2,000ms of biological time.

C. Creating the Spike Density Plots

To organize the spike time data, the data was binned in time and space to create a matrix where each entry contained the number of spikes that occurred during a specific window in time and a specific window along the vertical axis on the dentate gyrus. Each row of the matrix corresponded to the vertical position of the GC that elicited the spike. Each column corresponded to the time at which the spike was generated. Each matrix entry was the total of all the spikes that were generated in its corresponding spatial and temporal window. The temporal window, or bin, size was 1ms, and the spatial bin size was 0.05mm. With the vertical length of the dentate gyrus being defined as 10mm, there were a total of 200 rows in the matrix. With the simulations simulating 2000ms of biological time, there were 2000 columns. Because many granule cells could occupy a vertical extent of 0.05mm, multiple spikes can be generated for a given window in time and space.

Since each entry in the matrix corresponds to the number of spikes that occurred, simply dividing the entry by the width of the temporal or spatial window would provide an estimate of the mean temporal or spatial frequency at that spatiotemporal location, respectively. Because the window sizes were constant for all entries, this would simply scale the data. Color represents the relative number of spikes generated in each bin where red corresponds to the maximum number and blue corresponds to the minimum number. The color scale was normalized for each plot in order to accentuate how the activity varied among the simulations.

III. Results

A. Entorhinal Activation of Granule Cells

To understand how the spatial distribution and firing times of the EC cells could induce the spatiotemporal patterns generated by the granule cells, spike density plots were generated based on the EC input. The plots were constructed similarly to the GC plots with the exception of the location of the spike. For each EC spike time, a spike was plotted for each of its GC targets, based on the EC cell's spike time but each GC target's location.

Comparing the original EC cell plot and GC plot, no clear relationship between the input and output could be seen (Fig. 2). After convolving the data with a 2-D gaussian to smooth the data (σ_x = 3ms and σ_y = 0.15 ms, corresponding to three bin lengths each), clusters were seen in the EC cell plot that corresponded to clusters in the GC plot.

B. Varying the Perforation Point Distribution

Holding the axon terminal field constant at 1mm, arbitrary perforation point distributions were generated in addition to the anatomically derived distribution to test their effect on the activity of the granule cell population. The distributions would change the proportion of EC cells that would project to a region of the dentate gyrus. Dividing the dentate gyrus into quartiles, the "one-four" distribution would send 40%, 30%, 20%, and 10% of the input to the bottom, lower middle, upper middle, and top quartiles, respectively (Fig. 3). The "four-one" distribution is the reverse of "one-four" with more input in the top than the bottom. The "equal" distribution equally distributed the input across the entire dentate gyrus, while the "derived" distribution follows the anatomically-derived topography. The GC plots show that clusters still persist, although they appear in different locations and at different times across the different distribution types (Fig. 4). Each distribution type resulted in a similar number of total spikes being generated with a mean of 221,446 ± 1,791 spikes.

The total number of GC spikes generated per position in space was plotted by summing each row of the matrix data with the expectation that the distribution of activity across space would match the EC axon distribution (Fig. 3). However, the distribution of spikes across space was dependent on the number of granule cells that lay in each bin rather than the amount of input projecting to each bin. Applying the same analysis to the EC cell plots showed that the spatial distribution of their spikes followed the spatial distribution of granule cells even more closely (Fig. 3C).

The spatial distribution of granule cells also explained the dense activity that the EC cell plots were exhibiting in the upper half of the dentate gyrus. By normalizing each row of the matrix data by the number of granule cells that were located in each row, a causal EC cell cluster could be seen for the clusters found in the GC plot (Fig. 2). Normalizing the spike density data with the number of granule cells in each row converted the data from representing the total number of spikes fired in each bin to the average number of spikes fired per granule cell in each bin.

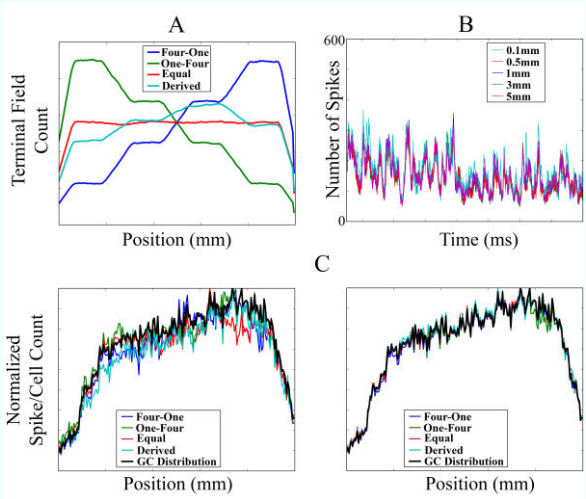

Figure 3. **A**. Demonstrating the various axon distributions tested. The number of projections in each spatial bin was counted. **B**. The number of spikes generated by GCs as a function of time. Each trace corresponds to a simulation using a different axon terminal field length. **C (left)**. The total number of spikes fired by the GCs at each vertical extent were normalized and plotted alongside the normalized number of GCs per bin. **C (right)**. The total number of spikes sent by the EC cells to the GCs per vertical extent were normalized and plotted alongside the normalized number of GCs per bin.

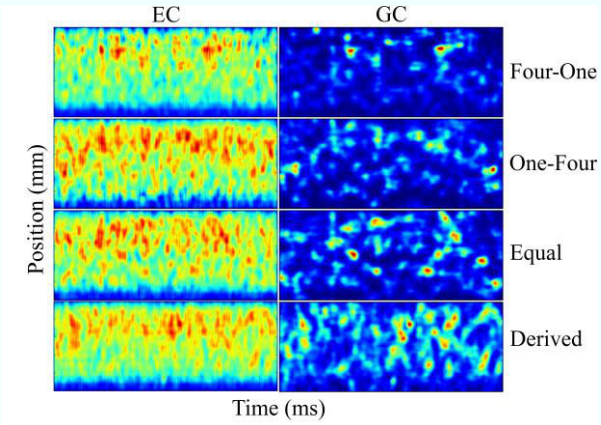

Figure 4. The EC cell activity and the GC activity resulting from the various axon distributions using an axon terminal field length of 1mm. The left column depicts the convolved EC cell data, and the right column shows the convolved GC data. (Not normalized by the granule cell distribution.)

C. Varying the Axon Terminal Fields of the EC Cells

The next set of experiments involved the variation of the axon terminal field. The axon terminal field lengths tested was 0.1, 0.5, 1, 3, and 5mm. The spike pattern generated by each EC cell was also kept constant across simulations. As the axon terminal field length increases, the cluster heights in the EC cell and GC data increase accordingly (Fig. 5).

Furthermore, the total number of spikes generated by the GCs per time was plotted by summing each column of the matrix data (Fig. 3B). What was observed is that regardless of the axon terminal field length, each simulation generated similar amount of spikes at each time.

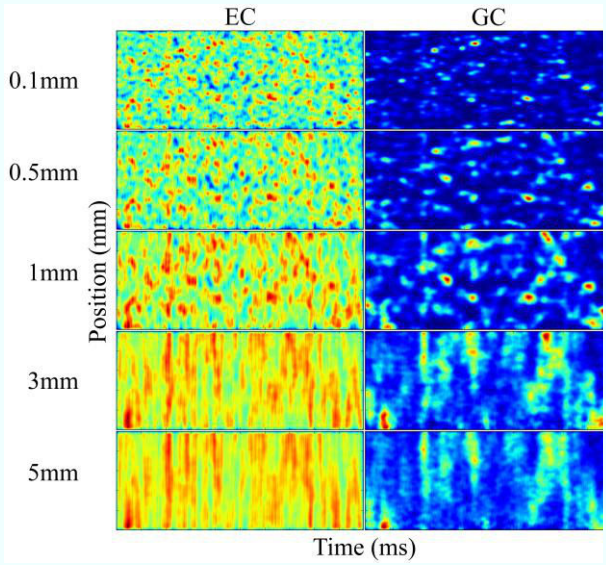

Figure 5. The EC cell and GC activity as axon terminal field length was varied. The left column represents the EC cell data and the right column represents the GC data. The cluster height is shown to increase as the axon terminal field length increases. The data was normalized using the granule cell distribution.

IV. Discussion

A. Postsynaptic Spine Density Dependent Spatial Activity

Fig. 3A shows the density of the presynaptic axons as a function of space. Although more input may have projected to a particular region, it was the number of GCs, or the postsynaptic density, that dictated the level of activity across the spatial extent. Because the spines per GC remained constant, the amount of spines available in a region depended on the number of GCs present which dictates the amount of input that can be sent to that region. Fig. 3 also shows that the anatomically-derived axon terminal field distribution and the granule cell distribution follow a similar shape. This allows each input to be sampled relatively equally.

B. Varying the Axon Terminal Fields

Each EC cell generated a random Poisson train independent of one another, and the inputs were sent to the dentate gyrus. The axon terminal field gave each input an area of influence that would overlap with the axon terminal fields of other inputs in space. Although the spike trains were independently generated and random, the axon terminal fields allowed multiple inputs to converge spatiotemporally creating local regions of higher activation. These were the clusters seen in the EC cell plots which in turn activated the corresponding GC population causing a similar cluster of activity. However, the spatiotemporal convergence of input did not always result in a GC cluster. Many clusters that appear in the EC cell plots do not result in clusters in the GC plots. This can be explained by the non-linear properties of neurons, most likely the afterhyperpolarization (AHP). Upon firing an action potential, the AHP would inhibit the neuron's ability to fire again until the AHP had diminished.

The total number of spikes per time did not change between the experiments. Increasing the axon terminal field length did not allow an EC cell to synapse with more granule cells although it could target more of them because of the finite number of postsynaptic spines and because each EC cell was competing with all the other overlapping input cells to synapse with a given target.

C. Implications of Topography

Assuming that the information encoded by each presynaptic neuron is unique, the axon distribution and terminal field will affect the ability for different inputs to converge and be integrated by a postsynaptic neuron. This gives the axon distribution a relevance that cannot be explored by investigating spiking activity alone. Looking at spatiotemporal activity in terms of number of spikes deemphasizes any unique information that an individual neuron may be encoding. Fig. 3B indicates that only approximately 0.2% (200 out of 100,000) of the population was firing at any millisecond. If a cluster of activity was repeated at a later point in time, the neurons that comprise that second cluster could be completely different from the first which would similarly change the information being encoded. Therefore, it is necessary to create a method to track the propagation of EC input as it is spatially gated via topography and temporally gated via neuronal integration. Tracing and relating the spatiotemporal convergence and divergence of individual input as it propagates through the trisynaptic loop may help clarify how the hippocampus is able to perform its memory-related duties.

Acknowledgment

Computation for the work described in this paper was supported by the University of Southern California Center for High-Performance Computing and Communications (www.usc.edu/hpcc).

References

[1] G. J. Yu, B. S. Robinson, P. J. Hendrickson, D. Song, and T. W. Berger, "Implementation of topographically constrained connectivity for a large-scale biologically realistic model of the hippocampus," *34th Annual International Conference of the IEEE EMBS*, 2012.

[2] C. L. Dolorfo and D. G. Amaral, "Entorhinal cortex of the rat: topographic organization of the cells of origin of the perforant path projection to the dentate gyrus," *The Journal of Comparative Neurology*, vol. 398, no. 1, pp. 25-48, Aug. 1998.

[3] N. T. Carnevale and M. L. Hines, "The NEURON book," Cambridge, UK: Cambridge University Press, 2006.

[4] P. J. Hendrickson, G.J. Yu, B. S. Robinson, D. Song, and T. W. Berger, "Toward a Large-Scale Biologically Realistic Model of the Hippocampus," *34th Annual International Conference of the IEEE EMBS*, 2012.

[5] V. Santhakumar, I. Aradi, and I. Soltesz, "Role of mossy fiber sprouting and mossy cell loss in hyperexcitability: A network model of the dentate gyrus incorporating cell types and axonal topography," *Journal of Neuroscience*. vol.93, no. 1, pp. 437-453, Jan. 2005.

[6] F. B. Gaarskjaer, "Organization of the mossy fiber system of the rat studied in extended hippocampi. I. Terminal area related to number of granule and pyramidal cells," *The Journal of comparative neurology*, vol. 178, no. 1, pp. 49-72, Mar. 1978.

[7] N. Tamamaki and Y. Nojyo, "Projection of the entorhinal layer II neurons in the rat as revealed by intracellular pressure-injection of neurobiotin," *Hippocampus*, vol. 3, no. 4, pp. 471-80, Oct. 1993.